

Signature of same-sign top pair production mediated by a nonuniversal Z' with QCD next-to-leading order accuracy at the LHC

Bo Hua Li,¹ Chong Sheng Li,^{1,2,*} Hai Tao Li,¹
Yong Chuan Zhan,¹ Yue Zhang,¹ and Jian Wang¹

¹*Department of Physics and State Key Laboratory of Nuclear Physics and Technology,
Peking University, Beijing 100871, China*

²*Center for High Energy Physics, Peking University, Beijing 100871, China*

(Dated: September 17, 2018)

Abstract

We present a detailed study of the same-sign top pair production mediated by a nonuniversal Z' including production and decay at the Large Hadron Collider (LHC) at the QCD next-to-leading order (NLO) level, using the narrow width approximation and helicity amplitudes method. We find that the QCD NLO corrections can loosen the constraint on the model parameters and reduce the dependence of the total cross sections on the factorization scale significantly. We also study the signature and backgrounds of the process at the NLO level. In order to suppress the backgrounds, we further investigate the difference between the production rates of the positively and negatively charged dilepton at the LHC, and find that the same-sign dilepton signal of the new physics could be discovered more easily. Besides, we also discuss the uncertainty from the parton distribution (PDF) at the NLO level.

PACS numbers: 14.65.Ha, 12.38.Bx, 11.30.Hv, 12.60.-i

*Electronic address: csli@pku.edu.cn

I. INTRODUCTION

Up to now, the top quark is the heaviest fundamental particle with a mass close to the electroweak (EW) symmetry breaking scale. Thus it would be more sensitive to the new physics beyond the standard model (SM). One way to study the new physics in the top quark sector is via the anomalous flavor-changing neutral-current (FCNC) couplings. Within the SM, the FCNC couplings are absent at tree level and occur through loop diagrams, which are further suppressed by the Glashow-Iliopoulos-Maiani mechanism [1]. However, in some new physics models, such as two Higgs doublet model [2], supersymmetric models [3], extra dimensions models [4], little Higgs models [5], and the Z' model [6, 7], the FCNC processes can occur at tree level, which may enhance the cross section to observable level.

Due to the small SM backgrounds for the same-sign dilepton final state, the same-sign top pair production is a good channel to study the FCNC couplings. There are already a lot of articles [8–14] discussing the same-sign top pair production process, and in most of there, the process is induced by the FCNC couplings. In general, these FCNC couplings can be divided into several types. One of the most important types involves a massive colorless vector boson, i.e., Z' , which is the gauge boson associated with additional $U(1)$ symmetries. The renormalizable FCNC interaction can be generally written as follows [6]

$$\mathcal{L} = \bar{u}\gamma^\mu(C_R P_R + C_L P_L)tZ'_\mu + h.c., \quad (1)$$

where C_R and C_L are the coupling strength and P_R and P_L are the projection operators. Because of the constraint from the $B_d - \bar{B}_d$ mixing [15], only the right-handed coupling is considered below.

Due to the high energy and luminosity at the Large Hadron Collider (LHC), abundant top quark events will be produced, so it is a good chance to investigate the same-sign top pair production process. In fact, from the measurements of the total cross sections, the CMS Collaboration has already set an upper limit on the parameters of the nonuniversal Z' [16, 17], and at the low Z' mass region the ATLAS Collaboration also gave a strong constraint [18]. However, both of these results are based on the leading-order (LO) calculations, which suffer from large-scale uncertainties and cannot match the expected experimental accuracy at hadron colliders. On the other hand, the backgrounds of the process can be further suppressed if we choose a more proper observable, as we will discuss below. In this paper, we present the complete QCD next-to-leading order (NLO) corrections to the same-sign top

pair production and decay (lepton channel) mediated by the nonuniversal Z' at the LHC and also investigate the signal and backgrounds of the process at the QCD NLO level. Note that associated production of a top quark and a Z' boson via this coupling was studied in Ref. [19] at NLO.

The arrangement of the paper is as follows. In Sec. II, we describe the method used in our calculation. In Sec. III we show the LO results for the process. In Sec. IV we present the details of the NLO calculations for the production and the decay processes. We give our numerical results in Sec. V, and Sec. VI is a brief summary.

II. NARROW WIDTH APPROXIMATION AND HELICITY AMPLITUDES METHOD

The narrow width approximation (NWA)[20, 21] is often used for a resonant process when the heavy resonance has a small decay width. If the resonance is a scalar, the total cross section can be separated into two parts, i.e., production and decay,

$$\begin{aligned}\sigma &= \frac{(2\pi)^7}{2s} \int_{q_{\min}^2}^{q_{\max}^2} dq^2 \int d\phi_p d\phi_d |\mathcal{M}_p(q^2)|^2 \left[(q^2 - M^2)^2 + (M\Gamma)^2 \right]^{-1} |\mathcal{M}_d(q^2)|^2 \\ &= \frac{(2\pi)^8}{4sM\Gamma} \int d\phi_p |\mathcal{M}_p(M^2)|^2 \int d\phi_d |\mathcal{M}_d(M^2)|^2,\end{aligned}\quad (2)$$

where M is the mass of the resonance and Γ is the decay width of the resonance. The \mathcal{M}_p , \mathcal{M}_d are the amplitudes of the resonance production and its decay, respectively.

However, in our case, the resonance is the top quark, so the process should be separated at the amplitude level. Since the intermediate top quark is on-shell [22, 23], its propagator can be written as

$$\frac{\not{q} + m_t}{(q^2 - m_t^2) + i(m_t\Gamma_t)} = \frac{u_+ \bar{u}_+ + u_- \bar{u}_-}{(q^2 - m_t^2) + i(m_t\Gamma_t)} \quad (3)$$

where u_+ and u_- denote the top quark spinors with positive and negative helicities, respectively. m_t is the top quark mass, and Γ_t is the total decay width of the top quark. Then Eq. (2) would be changed to the following form

$$\sigma = \frac{(2\pi)^8}{4sM\Gamma} \left(\int d\phi_p |\mathcal{M}_p^+|^2 \int d\phi_d |\mathcal{M}_d^+|^2 + \int d\phi_p |\mathcal{M}_p^-|^2 \int d\phi_d |\mathcal{M}_d^-|^2 \right), \quad (4)$$

where \mathcal{M}_p^\pm , \mathcal{M}_d^\pm are the helicity amplitudes of the same-sign top pair production and the top quark decay, respectively. It should be note that if $\int d\phi_p |\mathcal{M}_p^+|^2 = \int d\phi_p |\mathcal{M}_p^-|^2$ or

$\int d\phi_d |\mathcal{M}_d^+|^2 = \int d\phi_d |\mathcal{M}_d^-|^2$, after a polarization average factor $\frac{1}{2}$ is taken into account, Eq. (4) will be equivalent to Eq. (2).

We adopt the helicity amplitude method in our calculation. The massless spinors are denoted as [24]

$$|i^\pm\rangle \equiv u_\pm(k_i) = v_\mp(k_i), \quad \langle i^\pm| \equiv \bar{u}_\pm(k_i) = \bar{v}_\mp(k_i), \quad (5)$$

and massive spinors can be written as

$$\begin{aligned} u_\pm(p, M; \eta, p^b) &= \frac{(\not{p} + M) |\eta^\mp\rangle}{\langle p^{b\pm} | \eta^\mp\rangle}, & \bar{u}_\pm(p, M; \eta, p^b) &= \frac{\langle \eta^\mp | (\not{p} + M)}{\langle \eta^\mp | p^{b\pm}\rangle}, \\ v_\pm(p, M; \eta, p^b) &= \frac{(\not{p} - M) |\eta^\pm\rangle}{\langle p^{b\mp} | \eta^\pm\rangle}, & \bar{v}_\pm(p, M; \eta, p^b) &= \frac{\langle \eta^\pm | (\not{p} - M)}{\langle \eta^\pm | p^{b\mp}\rangle}, \end{aligned} \quad (6)$$

where p^b and η are two massless momenta, which fulfill the following conditions

$$p = p^b + \frac{M^2}{2p \cdot \eta} \eta, \quad p^2 = M^2, \quad (p^b)^2 = \eta^2 = 0. \quad (7)$$

Since the helicity of massive spinors have the following relations

$$\frac{\langle p^{b\mp} | \eta^\pm\rangle}{M} \bar{u}_\pm(p, M; p^b, \eta) = \bar{u}_\mp(p, M; \eta, p^b), \quad \frac{\langle p^{b\mp} | \eta^\pm\rangle}{M} v_\pm(p, M; p^b, \eta) = v_\mp(p, M; \eta, p^b), \quad (8)$$

we only present results for amplitudes of the same-sign top pair production with a (\dots, t^+, t^+) helicity configuration.

III. LEADING-ORDER RESULTS

At the LHC there is only one subprocess that contributes to the same-sign top pair production and decay (lepton channel) at the LO via the Z' FCNC couplings,

$$u u \longrightarrow t t \longrightarrow l^+ \nu b l^+ \nu b. \quad (9)$$

The corresponding Feynman diagrams are shown in Fig. 1, where the top quark is on-shell. Here and below we adopt the unitary gauge.

The LO helicity amplitudes for t -channel and u -channel same-sign top pair productions in four dimensions are

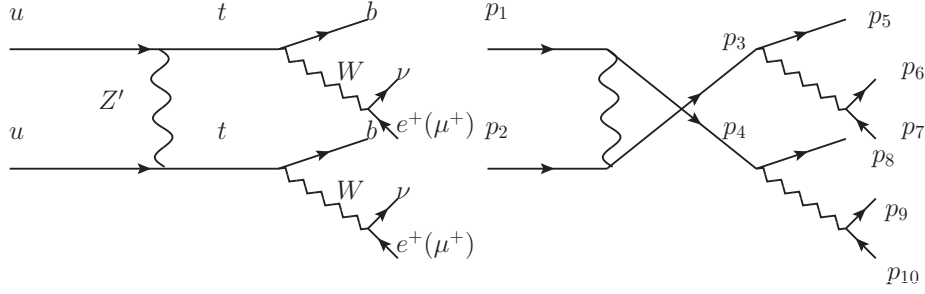


FIG. 1: The LO Feynman diagrams for the same-sign top pair production and decay at the leading order via the Z' FCNC couplings.

$$\begin{aligned} \mathcal{M}_t^{++++} &= \frac{2C_R^2}{(t - M_{Z'}^2)\langle\eta_3|p_3^b\rangle\langle\eta_4|p_4^b\rangle} \{ \langle p_2|p_1\rangle\langle\eta_4|p_1\rangle[p_1|\not{p}_3|\eta_3] + \langle p_2|p_1\rangle\langle\eta_4|p_2\rangle[p_2|\not{p}_3|\eta_3] \\ &\quad - m_t^2\langle p_2|p_1\rangle\langle\eta_4|\eta_3\rangle + \frac{m_t^4}{2M_{Z'}^2}\langle\eta_3|p_1\rangle\langle\eta_4|p_2\rangle \}, \end{aligned} \quad (10)$$

$$\begin{aligned} \mathcal{M}_u^{++++} &= \frac{-2C_R^2}{(u - M_{Z'}^2)\langle\eta_3|p_3^b\rangle\langle\eta_4|p_4^b\rangle} \{ \langle p_2|p_1\rangle\langle\eta_3|p_1\rangle[p_1|\not{p}_4|\eta_4] + \langle p_2|p_1\rangle\langle\eta_3|p_2\rangle[p_2|\not{p}_4|\eta_4] \\ &\quad - m_t^2\langle p_2|p_1\rangle\langle\eta_3|\eta_4\rangle + \frac{m_t^4}{2M_{Z'}^2}\langle\eta_4|p_1\rangle\langle\eta_3|p_2\rangle \}, \end{aligned} \quad (11)$$

and for the top quark decay

$$\mathcal{M}_{decay}^+ = -\frac{g^2 m_t U_{tb} \langle p_\nu | p_b \rangle [\eta_t | p_l]}{((p_t - p_b)^2 - M_W^2 + i M_W \Gamma_W) [\eta_t | p_t^b]}, \quad (12)$$

where $M_{Z'}$ and M_W are the masses of the Z' and W boson, respectively. Γ_W is the decay width of the W boson. U_{tb} is the CKM matrix element. g is the weak coupling. t and u are the Mandelstam variables, which are defined as

$$t = (p_1 - p_3)^2, \quad u = (p_1 - p_4)^2, \quad (13)$$

and p_t , p_b , p_ν , p_l are the four momentum of the top quark, bottom quark, neutrino and positron(anti-muon).

At the parton level, after the phase space integration, the LO cross sections are given by

$$\hat{\sigma}_B^{++} = \hat{\sigma}_t^{++} + \hat{\sigma}_u^{++} + \hat{\sigma}_{tu}^{++}, \quad (14)$$

where

$$\begin{aligned}\hat{\sigma}_t^{++} &= \frac{1}{2s} \int d\Gamma_2 \overline{\sum} |\mathcal{M}_t^{++++}|^2, \\ \hat{\sigma}_u^{++} &= \frac{1}{2s} \int d\Gamma_2 \overline{\sum} |\mathcal{M}_u^{++++}|^2, \\ \hat{\sigma}_{tu}^{++} &= -\frac{1}{s} \int d\Gamma_2 \overline{\sum} \text{Re}(\mathcal{M}_t^{++++} \mathcal{M}_u^{++++*}).\end{aligned}$$

The $\overline{\sum}$ means the colors of the final-state particles have been summed over and the colors and the spins of the initial-state particles have been averaged over. The top quark decay width for lepton channel at LO is

$$\Gamma_{t,l}^+ = \frac{1}{2m_t} \int d\Gamma_3 \overline{\sum} |\mathcal{M}_{decay}^+|^2. \quad (15)$$

The LO total cross section at hadron colliders is obtained by convoluting the partonic cross section with the parton distribution functions (PDFs) $G_{i/P}$ for the proton

$$\sigma^B = \sum_{ab} \int dx_1 dx_2 \left[G_{a/P_1}(x_1, \mu_f) G_{b/P_2}(x_2, \mu_f) \left(\sum_{i,j=+,-} \hat{\sigma}_B^{ij} \frac{\Gamma_{t,l}^i \Gamma_{t,l}^j}{\Gamma_t^2} \right)_{ab} \right], \quad (16)$$

where μ_f is the factorization scale.

IV. QCD NLO CORRECTIONS

The Feynman diagrams for the QCD NLO corrections to the same-sign top pair production and decay are shown in Figs. 12–14, which include both the virtual and the real corrections. The interface between the production and the decay process, at the NLO level, has been neglected, because their contributions are suppressed by $O(\frac{\Gamma_t}{m_t})$ [25–27].

We use the four-dimension helicity (FDH) scheme [28] in $n = 4 - 2\epsilon$ dimensions to regularize all the divergences. Moreover, for the real corrections, the two cutoff phase space slicing method [29] has been used to separate the infrared (IR) divergences.

A. Virtual corrections

The squared amplitudes of the virtual corrections are

$$\overline{|\mathcal{M}|^2}_{1-loop} = \overline{\sum} 2\text{Re}(\mathcal{M}^{loop} \mathcal{M}^{B*}) + \overline{\sum} 2\text{Re}(\mathcal{M}^{con} \mathcal{M}^{B*}), \quad (17)$$

where \mathcal{M}^{loop} are the amplitudes for the loop diagrams, and \mathcal{M}^{con} denotes the corresponding counterterms. Here and below the $\overline{\sum}$ means the colors and spins of the final-state particles have been summed over and the colors and spins of the initial-state particles have been averaged over.

The virtual corrections contain both UV and IR divergences. Since the process is induced by the electroweak-type FCNC couplings, the UV divergences can be cancelled by only introducing the following counterterms:

$$\delta Z_q = -\frac{\alpha_s}{3\pi} C_\epsilon \left\{ \frac{1}{\epsilon_{UV}} - \frac{1}{\epsilon_{IR}} \right\}, \quad (18)$$

$$\delta Z_t = -\frac{\alpha_s}{3\pi} C_\epsilon \left\{ \frac{1}{\epsilon_{UV}} + \frac{2}{\epsilon_{IR}} + 5 \right\}, \quad (19)$$

where $C_\epsilon = \Gamma(1 + \epsilon)[(4\pi\mu_r^2)/m_t^2]^\epsilon$. We define all the renormalization constants using the on-shell subtraction scheme.

In Eq. (17), all the UV divergences are canceled out, leaving the IR divergences and the finite terms. For the top quark production process, the IR divergence of the virtual corrections at the parton level can be factorized as [30, 31]

$$\begin{aligned} \hat{\sigma}_{pro}^{V(IR)} = & -\frac{\alpha_s C_\epsilon C_F}{\pi} \left\{ \left(\frac{1}{\epsilon^2} + \left(\frac{5}{2} - 2a_4 \right) \frac{1}{\epsilon} \right) \hat{\sigma}_t + \left(\frac{1}{\epsilon^2} + \left(\frac{5}{2} - 2a_3 \right) \frac{1}{\epsilon} \right) \hat{\sigma}_u - \right. \\ & \left. \left(\frac{1}{\epsilon^2} + \left(a_1 + \frac{a_2\beta}{2\sqrt{1-\beta}} - \frac{a_2}{\sqrt{1-\beta}} - 2a_3 - 2a_4 + \frac{5}{2} \right) \frac{1}{\epsilon} \right) \hat{\sigma}_{tu} \right\}, \end{aligned} \quad (20)$$

where

$$\begin{aligned} C_F &= \frac{4}{3}, \quad \beta = \frac{4m_t^2}{s}, \\ a_1 &= \ln\left(\frac{s}{m_t^2}\right), \quad a_2 = \ln\left(\frac{1 - \sqrt{1-\beta}}{1 + \sqrt{1-\beta}}\right), \\ a_3 &= \ln\left(\frac{m_t^2 - u}{m_t^2}\right), \quad a_4 = \ln\left(\frac{m_t^2 - t}{m_t^2}\right). \end{aligned} \quad (21)$$

For the top quark decay process, the IR divergence of the virtual corrections to the total cross section can be factorized as

$$\Gamma_{dec}^{V(IR)} = -\frac{\alpha_s C_\epsilon C_F}{2\pi} \left(\frac{1}{\epsilon^2} + \left(5 + 4 \ln\left(\frac{m_t^2}{2p_b \cdot p_t}\right) \right) \frac{1}{2\epsilon} \right) \Gamma_{t,l}, \quad (22)$$

where p_t and p_b are the top quark and bottom quark momentums, respectively. In order to cancel these divergences, we need to extract the IR divergences in the real corrections, which will be shown in the following subsection.

B. Real corrections

The real corrections consist of the radiations of an additional gluon $u u \rightarrow t t g$, or massless anti-quark in the final states, $g u \rightarrow t t \bar{u}$ as shown in Fig. 13. It should be noted that in our NLO calculations of the process, we include the contributions from the Z' on-shell production as the real corrections.

1. Real gluon emission

For real gluon emission, the phase space integration contains both soft and collinear singularities. We adopt the two cutoff phase space slicing method to isolate all the IR singularities [29], which introduces two small cutoff parameters δ_s and δ_c to divide the phase space into three parts. The soft cutoff δ_s separates the phase space into the soft region $E_5 \leq \delta_s \sqrt{s}/2$ and the hard region,

$$\hat{\sigma}^R = \hat{\sigma}^H + \hat{\sigma}^S. \quad (23)$$

Furthermore, the hard piece can be divided into two subregions by δ_c ,

$$\hat{\sigma}^H = \hat{\sigma}^{\overline{\text{HC}}} + \hat{\sigma}^{\text{HC}}. \quad (24)$$

The hard noncollinear part $\hat{\sigma}^{\overline{\text{HC}}}$ is finite and the phase space integration can be calculated numerically. For the soft region, in the limit that the energy of the emitted gluon becomes small, i.e. $E_5 \leq \delta_s \sqrt{s}/2$, the amplitude squared $\overline{|\mathcal{M}(uu \rightarrow tt + g)|^2}$ can be factorized into the Born amplitude squared times eikonal factors Φ_{eik}^i

$$\overline{|\mathcal{M}(uu \rightarrow tt + g)|^2} \xrightarrow{\text{soft}} (4\pi\alpha_s\mu_r^{2\epsilon}) \overline{\sum} (|\mathcal{M}_t|^2 \Phi_{\text{eik}}^a + |\mathcal{M}_u|^2 \Phi_{\text{eik}}^b + \text{Re}[2\mathcal{M}_t \mathcal{M}_u^*] \Phi_{\text{eik}}^c), \quad (25)$$

where the eikonal factor is given by

$$\Phi_{\text{eik}}^a = \frac{C_F}{2} \left\{ \frac{m_t^2 - t}{(p_1 \cdot p_5)(p_3 \cdot p_5)} + \frac{m_t^2 - t}{(p_2 \cdot p_5)(p_4 \cdot p_5)} - \frac{m_t^2}{(p_3 \cdot p_5)^2} - \frac{m_t^2}{(p_4 \cdot p_5)^2} \right\}, \quad (26)$$

$$\Phi_{\text{eik}}^b = \frac{C_F}{2} \left\{ \frac{m_t^2 - u}{(p_1 \cdot p_5)(p_4 \cdot p_5)} + \frac{m_t^2 - u}{(p_2 \cdot p_5)(p_3 \cdot p_5)} - \frac{m_t^2}{(p_3 \cdot p_5)^2} - \frac{m_t^2}{(p_4 \cdot p_5)^2} \right\}, \quad (27)$$

$$\begin{aligned} \Phi_{\text{eik}}^c = & \frac{C_F}{2} \left\{ \frac{s}{(p_1 \cdot p_5)(p_2 \cdot p_5)} - \frac{m_t^2 - t}{(p_1 \cdot p_5)(p_3 \cdot p_5)} - \frac{m_t^2 - u}{(p_1 \cdot p_5)(p_4 \cdot p_5)} - \frac{m_t^2 - u}{(p_2 \cdot p_5)(p_3 \cdot p_5)} \right. \\ & \left. - \frac{m_t^2 - t}{(p_2 \cdot p_5)(p_4 \cdot p_5)} + \frac{m_t^2}{(p_3 \cdot p_5)^2} + \frac{m_t^2}{(p_4 \cdot p_5)^2} \right\}. \quad (28) \end{aligned}$$

Moreover, the three-body phase space in the soft limit can also be factorized,

$$d\Gamma_3(uu \rightarrow tt + g) \xrightarrow{\text{soft}} d\Gamma_2(uu \rightarrow tt)dS. \quad (29)$$

Here dS is the integration over the phase space of the soft gluon which is given by

$$dS = \frac{1}{2(2\pi)^{3-2\epsilon}} \int_0^{\delta_s \sqrt{s}/2} dE_5 E_5^{1-2\epsilon} d\Omega_{2-2\epsilon}. \quad (30)$$

The parton level cross section in the soft region can be expressed as

$$\hat{\sigma}^S = \sum_i (4\pi\alpha_s\mu_r^{2\epsilon}) \int d\Gamma_2 \overline{\sum} |\mathcal{M}_B^i|^2 \int dS \Phi_{\text{eik}}^i. \quad (31)$$

Then, after the integration over the soft gluon phase space, the divergent parts of Eq.(31) become

$$\begin{aligned} \hat{\sigma}^S = & \frac{\alpha_s C_\epsilon C_F}{\pi} \left\{ \left(\frac{1}{\epsilon^2} + (1 - 2a_4 - 2 \ln(\delta_s)) \frac{1}{\epsilon} \right) \hat{\sigma}_t \right. + \\ & \left(\frac{1}{\epsilon^2} + (1 - 2a_3 - 2 \ln(\delta_s)) \frac{1}{\epsilon} \right) \hat{\sigma}_u - \left(\frac{1}{\epsilon^2} + \left(a_1 + \frac{a_2 \beta}{2\sqrt{1-\beta}} - \right. \right. \\ & \left. \left. \frac{a_2}{\sqrt{1-\beta}} - 2a_3 - 2a_4 + 1 - 2 \ln(\delta_s) \right) \frac{1}{\epsilon} \right) \hat{\sigma}_{tu} \left. \right\}. \quad (32) \end{aligned}$$

In the hard collinear region, $E_5 > \delta_s \sqrt{s}/2$ and $-\delta_c s < t_{i5} < 0$, the emitted hard gluon is collinear to one of the incoming partons. As a consequence of the factorization theorem[33, 34] the matrix element squared for $uu \rightarrow tt + g$ can be factorized into the product of the Born amplitude squared and the Altarelli-Parisi splitting function

$$\overline{\sum} |\mathcal{M}(uu \rightarrow tt + g)|^2 \xrightarrow{\text{collinear}} (4\pi\alpha_s\mu_r^{2\epsilon}) \overline{\sum} |\mathcal{M}^B|^2 \left(\frac{-2P_{qq}(z)}{zt_{15}} + \frac{-2P_{qq}(z)}{zt_{25}} \right), \quad (33)$$

where z denotes the fraction of the momentum of the incoming parton carried by $q(g)$, and the unregulated Altarelli-Parisi splitting function in our case is written explicitly as [32]

$$P_{qq}(z) = C_F \left(\frac{1+z^2}{1-z} \right). \quad (34)$$

Moreover, the three-body phase space can also be factorized in the collinear limit. For example, in the limit $-\delta_c s < t_{15} < 0$, it has the following form

$$d\Gamma_3(uu \rightarrow tt + g) \xrightarrow{\text{collinear}} d\Gamma_2(uu \rightarrow tt; s' = zs) \frac{(4\pi)^\epsilon}{16\pi^2 \Gamma(1-\epsilon)} dz dt_{15} [-(1-z)t_{15}]^{-\epsilon}. \quad (35)$$

Thus, after convoluting with the PDFs, the three-body cross section in the hard collinear region is given by

$$d\sigma^{HC} = d\hat{\sigma}^B \left[\frac{\alpha_s}{2\pi} \frac{\Gamma(1-\epsilon)}{\Gamma(1-2\epsilon)} \left(\frac{4\pi\mu_r^2}{s} \right)^\epsilon \right] \left(-\frac{1}{\epsilon} \right) \delta_c^{-\epsilon} \left[P_{qq}(z) G_{q/p}(x_1/z) G_{q/p}(x_2) \right. \\ \left. + P_{qq}(z) G_{q/p}(x_1) G_{q/p}(x_2/z) \right] \frac{dz}{z} \left(\frac{1-z}{z} \right)^{-\epsilon} dx_1 dx_2, \quad (36)$$

where $G_{q/p}(x)$ is the bare parton distribution function (PDF).

2. Massless antiquark emission

In addition to the real gluon emission, a second set of real emission corrections to the inclusive cross section for $pp \rightarrow tt$ at NLO involves the processes with an additional massless antiquark \bar{u} in the final state. Since the contributions from real massless \bar{u} emission contain initial state collinear singularities, we need to use the two cutoff phase space slicing method [29] to isolate these collinear divergences. The cross sections for the processes with an additional massless \bar{u} in the final state can be expressed as

$$d\sigma^{add} = \left\{ d\hat{\sigma}^{\bar{C}}(ug \rightarrow tt + \bar{u}) G_{u/p}(x_1) G_{g/p}(x_2) + \right. \\ d\hat{\sigma}^B \left[\frac{\alpha_s}{2\pi} \frac{\Gamma(1-\epsilon)}{\Gamma(1-2\epsilon)} \left(\frac{4\pi\mu_r^2}{s} \right)^\epsilon \right] \left(-\frac{1}{\epsilon} \right) \delta_c^{-\epsilon} P_{qg}(z) G_{u/p}(x_1/z) G_{g/p}(x_2) \\ \left. \frac{dz}{z} \left(\frac{1-z}{z} \right)^{-\epsilon} + (x_1 \leftrightarrow x_2) \right\} dx_1 dx_2, \quad (37)$$

where

$$P_{qg}(z) = \frac{1}{2} [z^2 + (1-z)^2]. \quad (38)$$

The $\hat{\sigma}^{\bar{C}}$ terms in Eq. (37) represents the noncollinear cross sections for the qg initiated processes which can be written in the form

$$d\hat{\sigma}^{\bar{C}} = \frac{1}{2s} \left\{ |\mathcal{M}(ug \xrightarrow{\text{noncollinear}} tt + \bar{u})|^2 \right\} d\bar{\Gamma}_3, \quad (39)$$

where $d\bar{\Gamma}_3$ is the three-body phase space in the noncollinear region. The other terms in Eq. (37) are the collinear singular cross sections.

3. Mass factorization

The soft divergences can be canceled out after adding the renormalized virtual corrections and the real corrections together. However, there still remain some collinear divergences which should be absorbed into a redefinition of the PDFs at the NLO [35, 36]. This procedure means that first we convolute the partonic cross section with the bare PDF $G_{\alpha/p}(x)$ and then use the renormalized PDF $G_{\alpha/p}(x, \mu_f)$ to replace $G_{\alpha/p}(x)$. In the modified minimal subtraction ($\overline{\text{MS}}$) convention the scale-dependent PDF $G_{\alpha/p}(x, \mu_f)$ is given by [29]

$$G_{\alpha/p}(x, \mu_f) = G_{\alpha/p}(x) + \sum_{\beta} \left(-\frac{1}{\epsilon} \right) \left[\frac{\alpha_s}{2\pi} \frac{\Gamma(1-\epsilon)}{\Gamma(1-2\epsilon)} \times \left(\frac{4\pi\mu_r^2}{\mu_f^2} \right)^{\epsilon} \right] \times \int_x^1 \frac{dz}{z} P_{\alpha\beta}(z) G_{\beta/p}(x/z). \quad (40)$$

Then the $\mathcal{O}(\alpha_s)$ expression for the remaining collinear contribution can be written in the following form

$$d\sigma^{coll} = d\hat{\sigma}^B \left[\frac{\alpha_s}{2\pi} \frac{\Gamma(1-\epsilon)}{\Gamma(1-2\epsilon)} \left(\frac{4\pi\mu_r^2}{s} \right)^{\epsilon} \right] \{ \tilde{G}_{u/p}(x_1, \mu_f) G_{u/p}(x_2, \mu_f) + \quad (41)$$

$$G_{u/p}(x_1, \mu_f) \tilde{G}_{u/p}(x_2, \mu_f) + 2 \left(\frac{A_1^{sc}(u \rightarrow ug)}{\epsilon} + A_0^{sc}(u \rightarrow ug) \right) G_{u/p}(x_1, \mu_f) G_{u/p}(x_2, \mu_f) \} dx_1 dx_2, \quad (42)$$

where

$$A_0^{sc} = A_1^{sc} \ln\left(\frac{s}{\mu_f^2}\right), \quad (43)$$

$$A_1^{sc}(q \rightarrow qg) = C_F(2 \ln \delta_s + 3/2), \quad (44)$$

$$\tilde{G}_{\alpha/p}(x, \mu_f) = \sum_{\beta} \int_x^{1-\delta_s \delta_{\alpha\beta}} \frac{dy}{y} G_{\beta/p}(x/y, \mu_f) \tilde{P}_{\alpha\beta}(y), \quad (45)$$

with

$$\tilde{P}_{\alpha\beta}(y) = P_{\alpha\beta}(y) \ln\left(\delta_c \frac{1-y}{y} \frac{s}{\mu_f^2}\right). \quad (46)$$

Then, the IR divergences of the real corrections can be written as

$$\hat{\sigma}_{pro}^{R(IR)} = \frac{\alpha_s C_\epsilon C_F}{\pi} \left\{ \left(\frac{1}{\epsilon^2} + \left(\frac{5}{2} - 2a_4 \right) \frac{1}{\epsilon} \right) \hat{\sigma}_t + \left(\frac{1}{\epsilon^2} + \left(\frac{5}{2} - 2a_3 \right) \frac{1}{\epsilon} \right) \hat{\sigma}_u - \left(\frac{1}{\epsilon^2} + \left(a_1 + \frac{a_2 \beta}{2\sqrt{1-\beta}} - \frac{a_2}{\sqrt{1-\beta}} - 2a_3 - 2a_4 + \frac{5}{2} \right) \frac{1}{\epsilon} \right) \hat{\sigma}_{tu} \right\}, \quad (47)$$

and now all the IR divergences from the virtual corrections in Eq. (20) are canceled by those in Eq. (47) exactly.

C. Real corrections for top quark decay

The real corrections for top quark decay only consist of the radiations of an additional gluon $t \rightarrow b W^+ g \rightarrow b e^+ \nu g$. Following the same procedure as for the real gluon emission of the production process, we can write down the soft and collinear parts easily

$$\begin{aligned}
d\hat{\sigma}_{soft} &= \frac{C_F \alpha_s}{2\pi} C_\epsilon \left\{ \left(\frac{1}{\epsilon^2} + \frac{(1 - 2 \ln(\delta_s))}{\epsilon} \right) + 2(\ln(\delta_s)^2 - \ln(\delta_s) + 2) - \frac{\pi^2}{6} \right\} d\hat{\sigma}_B \quad (48) \\
d\hat{\sigma}_{coll} &= \frac{C_F \alpha_s}{2\pi} C_\epsilon \left\{ 2 \ln \left(\frac{m_t^2}{2p_b \cdot p_t} \right) + 2 \ln(\delta_s) + \frac{3}{2} \right\} \frac{1}{\epsilon} - 2 \ln(\delta_c) \ln \left(\frac{m_t^2}{2p_b \cdot p_t} \right) \\
&\quad - 2 \ln(\delta_c) \ln(\delta_s) - \frac{3 \ln(\delta_c)}{2} - 2 \ln(\delta_s) \ln \left(\frac{m_t^2}{2p_b \cdot p_t} \right) - \ln^2 \left(\frac{m_t^2}{2p_b \cdot p_t} \right) \\
&\quad - \ln^2(\delta_s) - \frac{\pi^2}{3} + 3 \left\} d\hat{\sigma}_B.
\end{aligned}$$

And then the total IR divergent parts are

$$\Gamma_{dec}^{R(IR)} = \frac{\alpha_s C_\epsilon C_F}{2\pi} \left(\frac{1}{\epsilon^2} + (5 + 4 \ln(\frac{m_t^2}{2p_b \cdot p_t})) \frac{1}{2\epsilon} \right) \Gamma_t, \quad (49)$$

which cancel the IR divergence in Eq. (22).

V. NUMERICAL RESULTS

In this section we present all the numerical results. We fix the top mass $m_t = 172.5$ GeV and all the other SM input parameters are taken to be [37]:

$$\alpha_s(M_Z) = 0.118, \quad \alpha(M_Z) = 1/128.921, \quad M_W = 80.399 \text{ GeV}, \quad (50)$$

The CTEQ6.6 PDF set [38] is used throughout the calculations except for the backgrounds in which the CTEQ6L [38] is used. Both the renormalization and factorization scales are fixed to the top quark mass. We adopt the same cuts as in Ref. [16]

$$\begin{aligned}
p_T(j) &> 30 \text{ GeV}, \quad |\eta(j)| < 2.5, \\
|\eta(l)| &< 2.4, \quad \cancel{E}_T^{e\mu(ee, \mu\mu)} > 30(20) \text{ GeV}, \quad (51)
\end{aligned}$$

and the same-sign isolated leptons have $p_T(l) > 10$ GeV, one of which should have $p_T(l) > 20$ GeV.

A. QCD NLO Results

We can use the NLO corrections to update the LO results, but before that, we would show that it is reasonable to use the two cutoff phase space slicing method in our calculation. To use the two cutoff method, we introduce two small cutoffs δ_s and δ_c . For the total cross section without any kinematic cuts imposed, the δ_s dependence is shown in Fig.2 (left). If we impose the cuts on the parton, it would not be infrared safe. So we adopt the anti- k_t jet algorithm [39] and set $R = 0.7$ in our calculation. After all cuts imposed, the δ_s dependence is shown in Fig.2 (right). Here, we only show the electron final state as an example. The soft, collinear and the noncollinear contributions individually depend strongly on the cutoffs. However, the cutoff dependence in the two contributions ($\sigma^S + \sigma^{coll}$ and $\sigma^{\overline{HC}} + \sigma^{\overline{C}}$) nearly cancel each other, so the final results for σ^{NLO} are almost independent of the cutoffs.

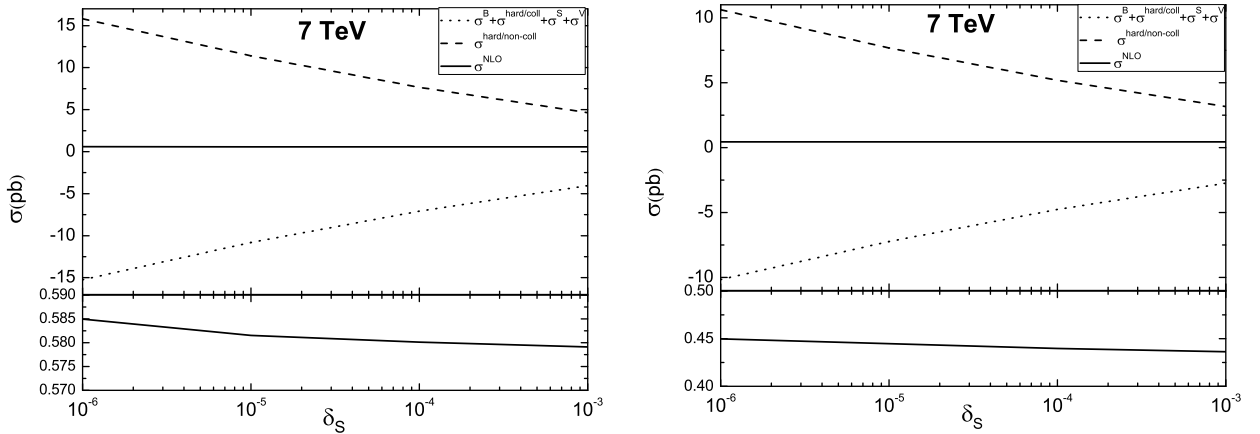


FIG. 2: Inclusive total cross sections for $pp \rightarrow tt \rightarrow e^+e^+ + 2jets + \cancel{E} + X$ at the LHC as a function of δ_s in the phase space slicing treatment. The left and right figures are shown for the cases without and with cuts, respectively. Here, $C_R = 2$ and the δ_c is chosen to be $\delta_c = \delta_s/50$.

As mentioned in the introduction, the CMS Collaboration has set a limit on the parameter C_R and $M_{Z'}$ based on the LO calculations. According to our numerical result, the NLO corrections can loosen this constraint but this kind of Z' still cannot explain the top quark forward-backward asymmetry as shown in Fig. 3.

In Fig.4, we plot the total cross section and the K factor, defined as σ_{NLO}/σ_{LO} , as the function of the Z' boson mass. Because of the large negative contributions from the interference between the loop corrections and the Born amplitudes, the NLO corrections

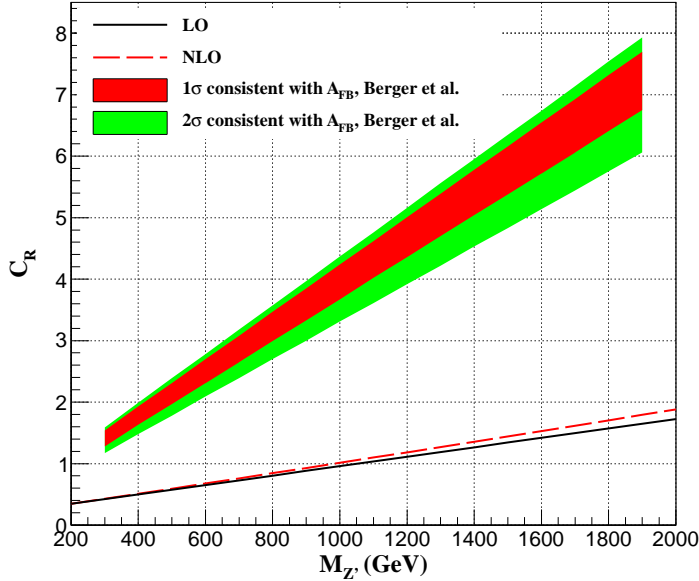


FIG. 3: Constraint line (solid) from the CMS collaboration. Considering the NLO corrections, we have a new constraint line (dashed), which loosens the constraint on the model parameters.

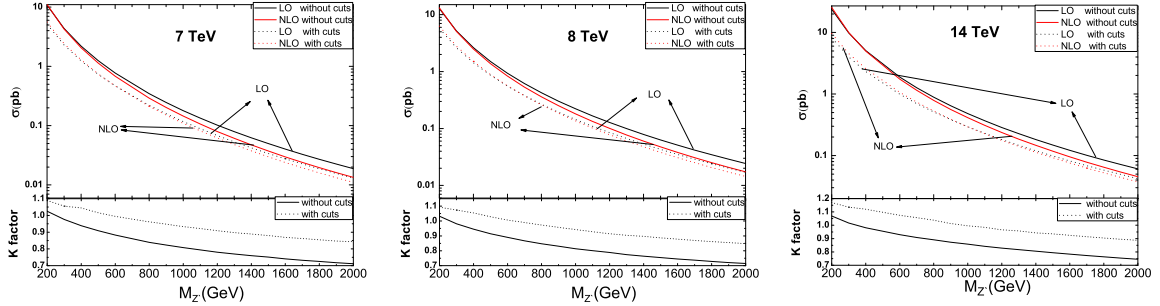


FIG. 4: The total cross section and the K factor as the function of the $M_{Z'}$ at the LHC with $C_R = 1$.

reduce the cross section. We can see that the QCD NLO corrections are more significant for larger Z' boson mass.

If the total cross section is fixed to be a certain value, for example 1 pb, we can also plot the C_R parameter as the function of the Z' boson mass, as shown in Fig.5. It is easy to find that, the curve in Fig.5 is nearly a straight line, when Z' boson mass is larger than about 500 GeV. This means the numerical results can be written in the following form if the Z'

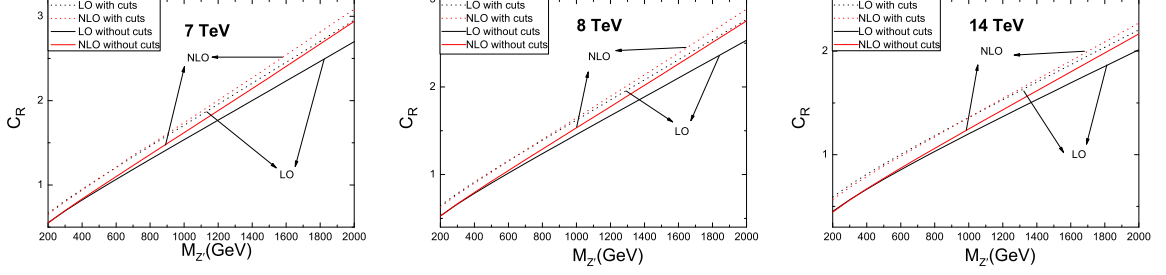


FIG. 5: The right-handed coupling C_R versus the Z' mass. Here we fix the total cross sections to be 1 pb.

decay width($\Gamma_{Z'}$) is fixed to a certain value,

$$\sigma = A \frac{C_R^4}{(M'_Z/\text{GeV} + b)^4}, \quad (52)$$

where A and b are two parameters that depend on the cuts and the center-of-mass Energy (E_{CM}). Then, when Z' boson mass is large enough, i.e., for $E_{CM} = 7, 8$ TeV, $M_{Z'} > 600$ GeV and for $E_{CM} = 14$ TeV, $M_{Z'} > 800$ GeV. Since Z' may have other unknown decay channels [6], its total decay width should be larger than the decay width to $u\bar{t}$ and $\bar{u}t$. Here we set $\Gamma_{Z'} = \Gamma_{Z' \rightarrow u\bar{t}, \bar{u}t}$ with $C_R = 2$, then our results can be present as follows:

without cuts:

$$\begin{aligned} \sigma_{7TeV}^{LO}(M'_Z) &= \frac{5.41975 \times 10^{11} \text{pb } C_R^4}{(M'_Z/\text{GeV} + 316.043)^4}, & \sigma_{7TeV}^{NLO}(M'_Z) &= \frac{3.38221 \times 10^{11} \text{pb } C_R^4}{(M'_Z/\text{GeV} + 236.603)^4} \\ \sigma_{8TeV}^{LO}(M'_Z) &= \frac{7.2622 \times 10^{11} \text{pb } C_R^4}{(M'_Z/\text{GeV} + 341.16)^4}, & \sigma_{8TeV}^{NLO}(M'_Z) &= \frac{4.52627 \times 10^{11} \text{pb } C_R^4}{(M'_Z/\text{GeV} + 257.476)^4} \\ \sigma_{14TeV}^{LO}(M'_Z) &= \frac{2.10819 \times 10^{12} \text{pb } C_R^4}{(M'_Z/\text{GeV} + 438.537)^4}, & \sigma_{14TeV}^{NLO}(M'_Z) &= \frac{1.35683 \times 10^{12} \text{pb } C_R^4}{(M'_Z/\text{GeV} + 342.761)^4}, \end{aligned}$$

with cuts:

$$\begin{aligned} \sigma_{7TeV}^{LO}(M'_Z) &= \frac{4.13553 \times 10^{11} \text{pb } C_R^4}{(M'_Z/\text{GeV} + 368.894)^4}, & \sigma_{7TeV}^{NLO}(M'_Z) &= \frac{3.13669 \times 10^{11} \text{pb } C_R^4}{(M'_Z/\text{GeV} + 303.198)^4}, \\ \sigma_{8TeV}^{LO}(M'_Z) &= \frac{5.6705 \times 10^{11} \text{pb } C_R^4}{(M'_Z/\text{GeV} + 405.522)^4}, & \sigma_{8TeV}^{NLO}(M'_Z) &= \frac{4.28346 \times 10^{11} \text{pb } C_R^4}{(M'_Z/\text{GeV} + 332.548)^4}, \\ \sigma_{14TeV}^{LO}(M'_Z) &= \frac{1.82195 \times 10^{12} \text{pb } C_R^4}{(M'_Z/\text{GeV} + 571.211)^4}, & \sigma_{14TeV}^{NLO}(M'_Z) &= \frac{1.39929 \times 10^{12} \text{pb } C_R^4}{(M'_Z/\text{GeV} + 474.653)^4}. \end{aligned} \quad (53)$$

In order to check these functions, we plot them in Fig. 6 and find that they are fitted well with the numerical results of the total cross sections.

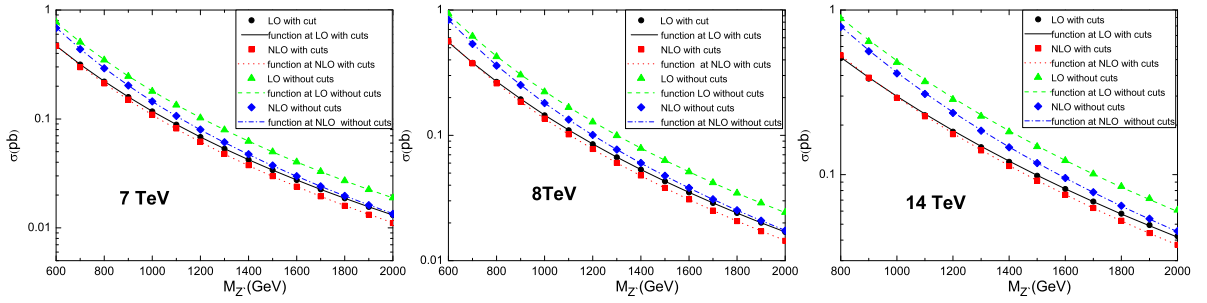


FIG. 6: The total cross sections predicted by Eq.(53) (curve) and the numerical results (scatter points). C_R was chosen to be 1 here.

In Fig. 7 we show the scale dependence of the LO and NLO total cross section at the LHC with different parameter values. We can see that, in all these cases, when the scale(μ) varies from $0.5m_t$ to $2m_t$, the NLO corrections reduce the factorization scale(μ_f) dependence significantly. And at the NLO level, the total scale dependence ($\mu_f = \mu_r = \mu$) will increase when M_Z' increase or E_{CM} decrease. Since there is no renormalization scale(μ_r) dependence at LO, the scale dependence is just the factorization scale dependence at LO, which is also the reason why the total scale dependence ($\mu_f = \mu_r = \mu$) is not reduced significantly at NLO.

We also discuss the uncertainties from the PDF [40] as shown in Fig. 8. According to our results, the PDF uncertainties are 3% – 4%, which are almost independent of E_{CM} and M_Z' .

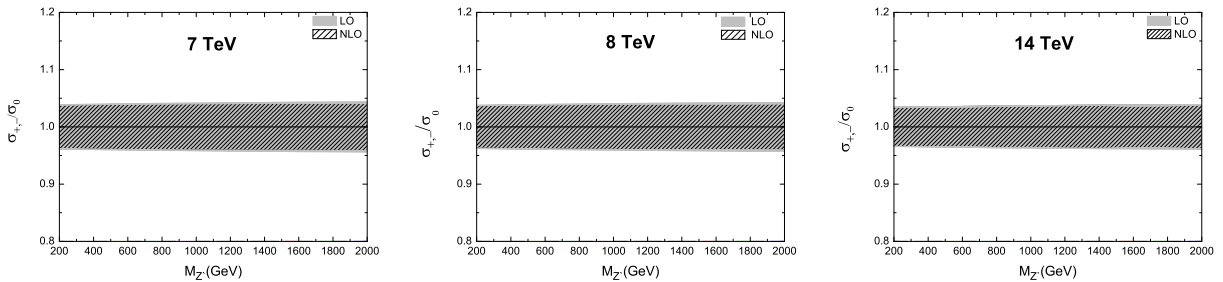


FIG. 8: PDF uncertainties with different E_{CM} and Z' mass at the LHC with $C_R = 1$. σ_+ and σ_- are the upper and lower limits of the total cross sections respectively. σ_0 is the central value of the total cross sections.

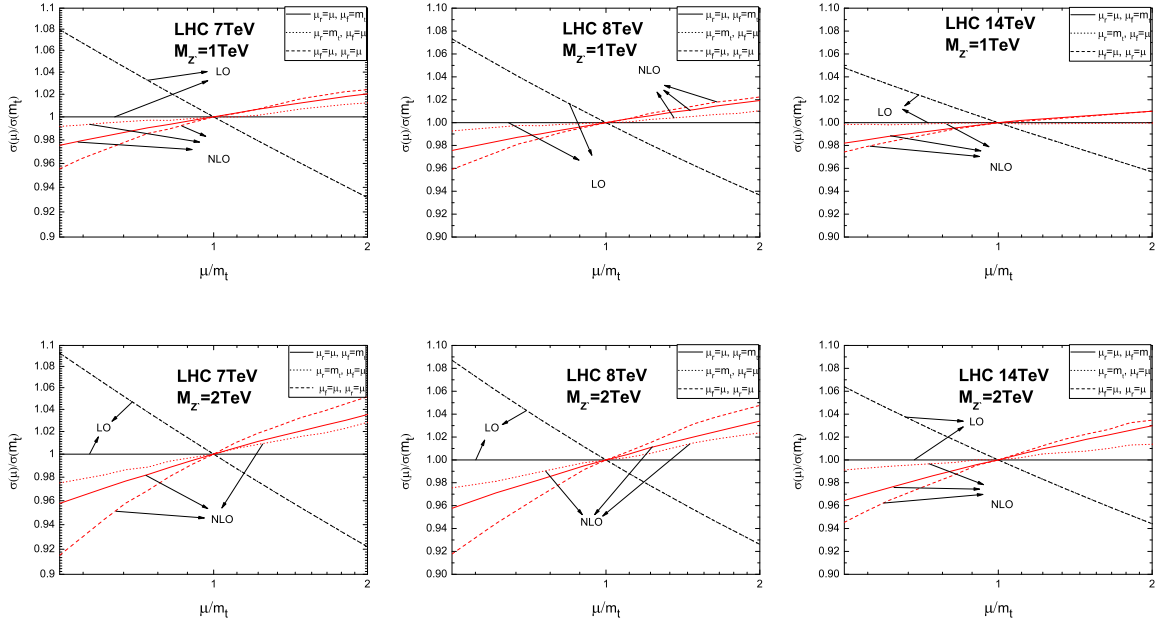


FIG. 7: Scale dependence of the total cross sections at the LHC with $C_R = 1$. The black line represents the LO result, while the red one represents the NLO result.

After including the scale uncertainty (running from $0.5m_t$ to $2m_t$) and the PDF uncertainties, some typical numerical results of the LO and NLO total cross sections are shown in Table I, assuming $C_R = 1$. It can be seen that the QCD NLO corrections can reduce the theoretical uncertainties.

	7TeV	8TeV	14TeV
LO ($M_{Z'} = 1TeV$)	$179.58^{+14.28}_{-12.26} \pm 7.48$	$222.3^{+16.27}_{-14.08} \pm 9.04$	$480.58^{+22.98}_{-20.69} \pm 17.75$
NLO ($M_{Z'} = 1TeV$)	$145.03^{+3.51}_{-6.45} \pm 5.98$	$180.87^{+4.05}_{-7.38} \pm 7.27$	$412.32^{+4.12}_{-10.57} \pm 14.68$
LO ($M_{Z'} = 2TeV$)	$18.86^{+1.75}_{-1.47} \pm 0.83$	$24.29^{+2.11}_{-1.79} \pm 1.04$	$60.82^{+3.88}_{-3.39} \pm 2.37$
NLO ($M_{Z'} = 2TeV$)	$13.41^{+0.69}_{-1.13} \pm 0.58$	$17.36^{+0.83}_{-1.42} \pm 0.73$	$45.34^{+1.57}_{-2.47} \pm 1.73$

TABLE I: The LO and the NLO total total cross sections (in fb) for the same-sign top pair production mediated by a nonuniversal Z' with different E_{CM} and Z' mass. Here the first and second errors denote the scale and PDF uncertainties, respectively.

B. Signature and background

The cleanest decay mode of the same-sign top pair is to same-sign leptons. The main background to this signal comes from the $t\bar{t}$ (when the events are selected without b-tagging), $t\bar{t} + Z$ and $t\bar{t} + W$ productions, as discussed in Refs. [16, 17, 41]. In order to suppress this background, we investigate the difference between the production rate of the positively and negatively charged dilepton

$$\Delta\sigma = \sigma_{++} - \sigma_{--}, \quad (54)$$

where σ_{++} and σ_{--} are the total cross sections of the positively and negatively charged same-sign dilepton production processes, respectively. The negative same-sign leptons can be produced through the process, $\bar{u}\bar{u} \rightarrow \bar{t}\bar{t} \rightarrow l^-\nu\bar{b}l^-\nu\bar{b}$. Since the LHC is a proton-proton collider, for the same-sign top pair production process, the σ_{--} is much smaller than the σ_{++} as shown in Fig.9(left) because of the difference of the densities between u and \bar{u} . However, for the $t\bar{t}$ and $t\bar{t} + Z$ backgrounds, in principle, the $\Delta\sigma$ should vanish. Thus, the dominant SM backgrounds are $pp \rightarrow Wt\bar{t}$, $pp \rightarrow WWqq$ ($q = u, d, c, s$), and $pp \rightarrow WZqq$ when one lepton is undetected [14]. But from the Fig.9(right), these backgrounds are also strongly suppressed (about 50%) for the $\Delta\sigma$. Besides, to further suppress these backgrounds, the double b-tag and additional cuts $m_{jj} < 60$ GeV or $m_{jj} > 100$ GeV are required. And we give some typical numerical results of the $\Delta\sigma$ for the signal (with $M'_Z = 1$ TeV and $C_R = 1$) and the backgrounds in Table II. We also show the 5σ and 3σ discovery limits on C_R and $M_{Z'}$ in Fig.10 and set $\Gamma_{Z'} = \Gamma_{Z' \rightarrow u\bar{t}, \bar{u}t}$ with $C_R = 2$ here. We can see that, when going from 8 to 14 TeV at LHC, the detection capability of the 8 TeV LHC with 10fb^{-1} is already good enough to study the same-sign top pair process. This is caused by the following: (1) The background and the signal increase almost at the same rates. (2) Since the cross sections are proportional to C_R^4 for a given value of $M_{Z'}$, the constraints on the C_R are not strong by the cross section.

Process	signal(NLO)	$Wt\bar{t}$	$WWqq$	$WZqq$
$E_{CM} = 8 \text{ TeV}$	32.18	0.0064	0.0003	0.0014
$E_{CM} = 14 \text{ TeV}$	69.03	0.0131	0.0005	0.0025

TABLE II: $\Delta\sigma$ of the signal and backgrounds (in fb) after all the cuts, assuming $M'_Z = 1\text{TeV}$ and $C_R = 1$.

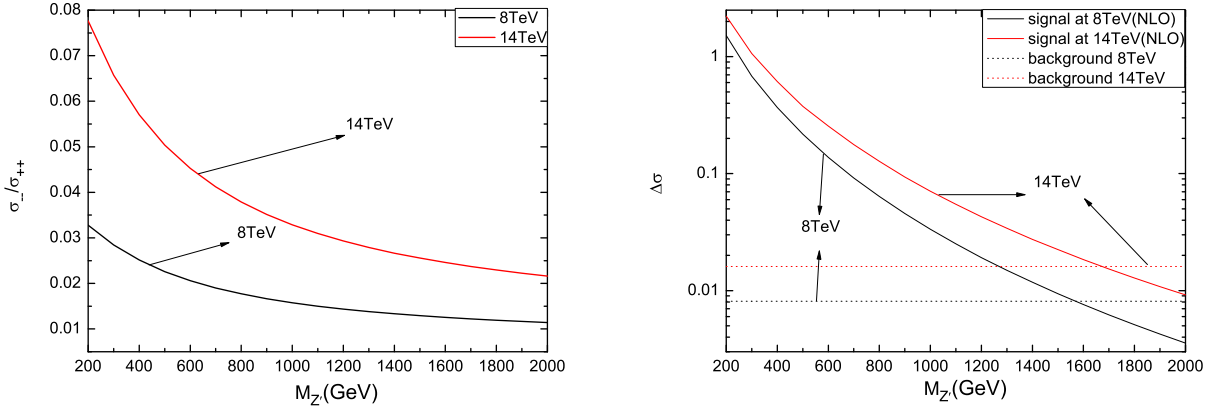


FIG. 9: Ratio between σ_{--} and σ_{++} and $\Delta\sigma$ as a function of M'_Z at the LHC with $E_{CM} = 8 \text{ TeV}$ and $E_{CM} = 14 \text{ TeV}$ and $C_R = 1$ for the same-sign top pair production process.

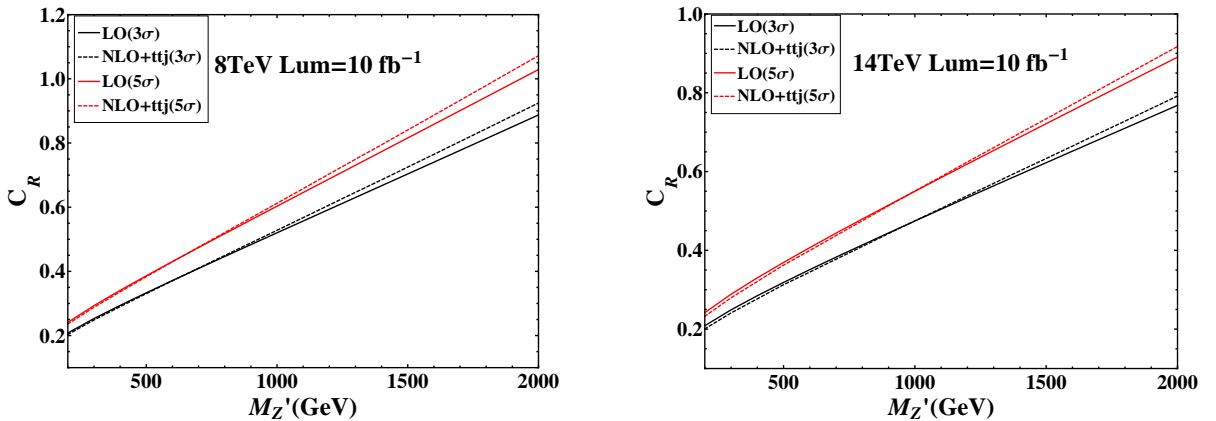


FIG. 10: The 5σ (upper two lines) and 3σ (lower two lines) discovery limits on C_R and M'_Z .

The observable defined in Eq. (54) can also be used in other same-sign top pair process, such as those discussed in Refs. [8–14].

In Fig. 11 we show the dependence of the differential distributions on missing energy (\cancel{E}_T) and H_T (scalar sum of final-state visible particle transverse momenta). From Fig. 11 we can see that QCD NLO corrections reduce significantly the distributions of missing energy and H_T in the ranges of 70-200 GeV and 200-600 GeV, respectively. This is due to the fact that the real corrections have additional jet emissions.

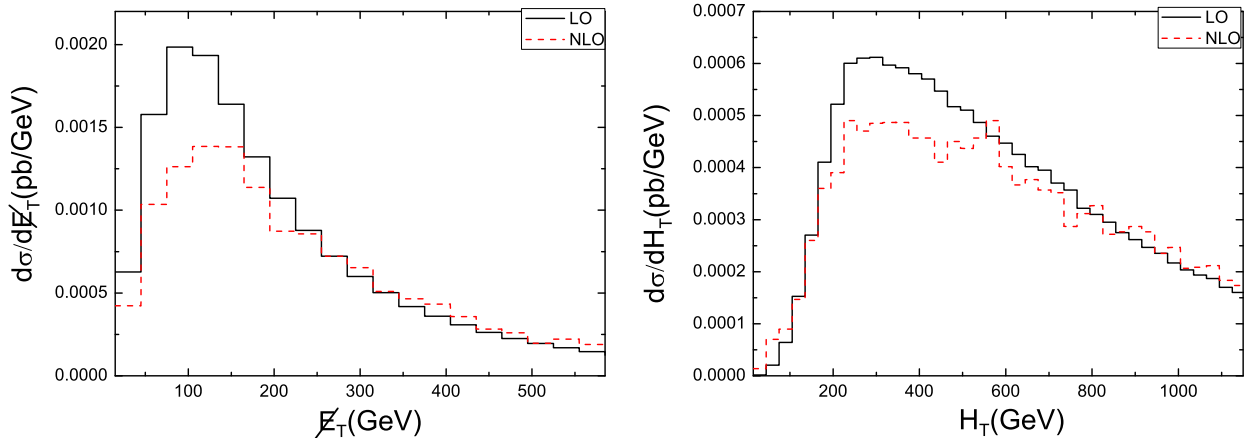


FIG. 11: \cancel{E}_T and H_T distributions at the LHC with $\sqrt{S} = 14$ TeV. Here, we assume $C_R = 1$ and $M_{Z'} = 1$ TeV.

VI. CONCLUSIONS

In conclusion we have investigated the complete QCD NLO corrections to the same-sign top pair production mediated by the nonuniversal Z' including production and decay at the LHC. Our results show that the QCD NLO corrections reduce the total cross sections by more than 10% for Z' boson mass greater than 500 GeV and loosen the constraint on the model parameters when comparing with the CMS Collaboration results. We also show that the total cross sections, including the QCD NLO corrections, can be expressed as the explicit functions of the model parameters C_R and $M_{Z'}$ generally. These functions may help experimentalists to quickly estimate the cross sections in their studies. Besides, the NLO corrections reduce the dependence of the total cross sections on the factorization scale significantly. We also study the signature and backgrounds of the process at the NLO level. Using the difference between the σ_{++} and the σ_{--} as shown in Eq.(54), we show that, in

principle, the $t\bar{t}$ and $t\bar{t} + Z$ backgrounds can be totally excluded, and the same-sign dilepton signal of the new physics could be discovered more easily.

Acknowledgments

This work was supported in part by National Nature Science Foundation of China, under Grants No. 11021092, No. 10975004 and No. 11135003.

-
- [1] S. L. Glashow, J. Iliopoulos and L. Maiani, Phys. Rev. D **2** (1970) 1285.
 - [2] T. P. Cheng and M. Sher, Phys. Rev. D **35** (1987) 3484; M. E. Luke and M. J. Savage, Phys. Lett. B **307** (1993) 387; D. Atwood, L. Reina and A. Soni, Phys. Rev. D **55** (1997) 3156; S. Bejar, J. Guasch and J. Sola, Nucl. Phys. B **600** (2001) 21.
 - [3] C. S. Li, R. J. Oakes and J. M. Yang, Phys. Rev. D **49** (1994) 293 [Erratum-ibid. D **56** (1997) 3156]; J. L. Lopez, D. V. Nanopoulos and R. Rangarajan, Phys. Rev. D **56** (1997) 3100; G. M. de Divitiis, R. Petronzio and L. Silvestrini, Nucl. Phys. B **504** (1997) 45; J. M. Yang, B. L. Young and X. Zhang, Phys. Rev. D **58** (1998) 055001; J. Guasch and J. Sola, Nucl. Phys. B **562** (1999) 3; G. Eilam, A. Gemintern, T. Han, J. M. Yang and X. Zhang, Phys. Lett. B **510** (2001) 227; J. j. Cao, Z. h. Xiong and J. M. Yang, Phys. Rev. Lett. **88** (2002) 111802; J. J. Liu, C. S. Li, L. L. Yang and L. G. Jin, Phys. Lett. B **599** (2004) 92.
 - [4] H. Davoudiasl and T. G. Rizzo, Phys. Lett. B **512** (2001) 100; P. M. Aquino, G. Burdman and O. J. P. Eboli, Phys. Rev. Lett. **98** (2007) 131601; S. Casagrande, F. Goertz, U. Haisch, M. Neubert and T. Pfoh, JHEP **0810** (2008) 094; J. Gao, C. S. Li, X. Gao and Z. Li, Phys. Rev. D **78** (2008) 096005.
 - [5] H. Hong-Sheng, Phys. Rev. D **75** (2007) 094010; X. Wang, Y. Zhang, H. Jin and Y. Xi, Nucl. Phys. B **810** (2009) 226; X. F. Han, L. Wang and J. M. Yang, arXiv:0903.5491 [hep-ph].
 - [6] S. Jung, H. Murayama, A. Pierce and J. D. Wells, Phys. Rev. D **81**, 015004 (2010) [arXiv:0907.4112 [hep-ph]].
 - [7] M. I. Gresham, I. -W. Kim and K. M. Zurek, Phys. Rev. D **84**, 034025 (2011) [arXiv:1102.0018 [hep-ph]].
 - [8] F. Larios and F. Penunuri, J. Phys. G G **30**, 895 (2004) [hep-ph/0311056].

- [9] S. Bar-Shalom and A. Rajaraman, Phys. Rev. D **77**, 095011 (2008) [arXiv:0711.3193 [hep-ph]].
- [10] S. P. Martin, Phys. Rev. D **78**, 055019 (2008) [arXiv:0807.2820 [hep-ph]].
- [11] H. Zhang, E. L. Berger, Q. -H. Cao, C. -R. Chen and G. Shaughnessy, Phys. Lett. B **696**, 68 (2011) [arXiv:1009.5379 [hep-ph]].
- [12] S. K. Gupta, arXiv:1011.4960 [hep-ph].
- [13] E. L. Berger, Q. -H. Cao, C. -R. Chen, C. S. Li and H. Zhang, Phys. Rev. Lett. **106**, 201801 (2011) [arXiv:1101.5625 [hep-ph]].
- [14] J. Gao, C. S. Li, X. Gao and Z. Li, Phys. Rev. D **78**, 096005 (2008) [arXiv:0808.3302 [hep-ph]].
- [15] Q. -H. Cao, D. McKeen, J. L. Rosner, G. Shaughnessy and C. E. M. Wagner, Phys. Rev. D **81**, 114004 (2010) [arXiv:1003.3461 [hep-ph]].
- [16] S. Chatrchyan *et al.* [CMS Collaboration], JHEP **1108**, 005 (2011) [arXiv:1106.2142 [hep-ex]].
- [17] S. Chatrchyan *et al.* [CMS Collaboration], arXiv:1205.3933 [hep-ex].
- [18] G. Aad *et al.* [ATLAS Collaboration], Phys. Rev. D **88**, 032004 (2012) [arXiv:1201.1091 [hep-ex]].
- [19] J. Adelman, J. Ferrando and C. D. White, arXiv:1206.5731 [hep-ph].
- [20] N. Kauer, Phys. Lett. B **649**, 413 (2007) [hep-ph/0703077].
- [21] C. F. Uhlemann and N. Kauer, Nucl. Phys. B **814**, 195 (2009) [arXiv:0807.4112 [hep-ph]].
- [22] K. Melnikov and M. Schulze, JHEP **0908**, 049 (2009) [arXiv:0907.3090 [hep-ph]].
- [23] J. M. Campbell, R. K. Ellis and F. Tramontano, Phys. Rev. D **70**, 094012 (2004) [hep-ph/0408158].
- [24] S. Badger, J. M. Campbell and R. K. Ellis, JHEP **1103**, 027 (2011) [arXiv:1011.6647 [hep-ph]].
- [25] V. S. Fadin, V. A. Khoze and A. D. Martin, Phys. Lett. B **320** (1994) 141 [hep-ph/9309234].
- [26] V. S. Fadin, V. A. Khoze and A. D. Martin, Phys. Rev. D **49**, 2247 (1994).
- [27] K. Melnikov and O. I. Yakovlev, Phys. Lett. B **324**, 217 (1994) [hep-ph/9302311].
- [28] Z. Bern, A. De Freitas, L. J. Dixon and H. L. Wong, Phys. Rev. D **66**, 085002 (2002) [hep-ph/0202271].
- [29] B. W. Harris and J. F. Owens, Phys. Rev. D **65**, 094032 (2002).
- [30] A. Denner, Fortsch. Phys. **41** 307 (1993).
- [31] R. K. Ellis and G. Zanderighi, JHEP **0802** 002 (2008).
- [32] G. Altarelli and G. Parisi, Nucl. Phys. B **126**, 298 (1977).
- [33] J. C. Collins, D. E. Soper and G. Sterman, Nucl. Phys. B **261**, 104 (1985).

- [34] G. T. Bodwin, Phys. Rev. **D 31**, 2616 (1985);
- [35] G. Altarelli, R.K. Ellis, and G. Martinelli, Nucl. Phys. **B 157**, 461 (1979)
- [36] J.C. Collins, D.E. Soper and G. Sterman, Adv. Ser. Direct. High Energy Physics.5, 1 (1988)
- [37] K. Nakamura *et al.* [Particle Data Group], J. Phys. G **37**, 075021 (2010).
- [38] J. Pumplin, D. R. Stump, J. Huston, H. L. Lai, P. M. Nadolsky and W. K. Tung, JHEP **0207** (2002) 012.
- [39] M. Cacciari, G. P. Salam and G. Soyez, JHEP **0804**, 063 (2008) [arXiv:0802.1189 [hep-ph]].
- [40] G. Watt, JHEP **1109**, 069 (2011) [arXiv:1106.5788 [hep-ph]].
- [41] S. Chatrchyan *et al.* [CMS Collaboration], JHEP **1106**, 077 (2011) [arXiv:1104.3168 [hep-ex]].

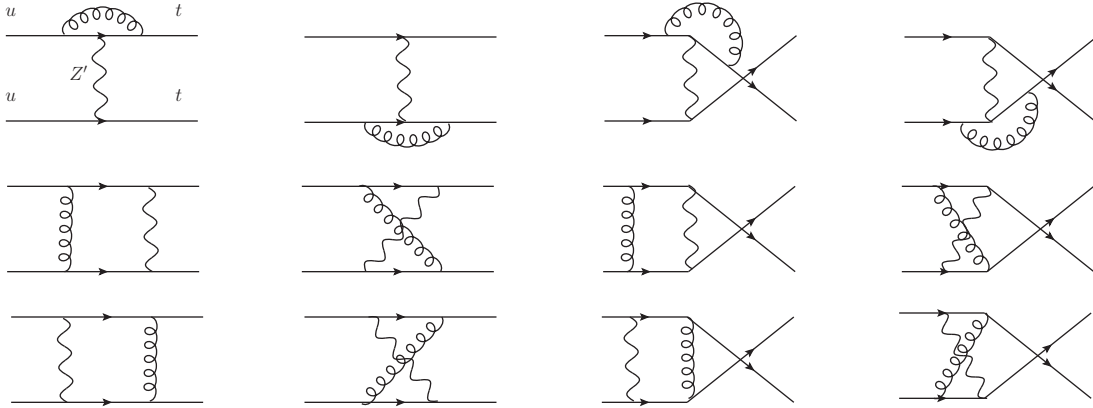


FIG. 12: 1-loop Feynman diagrams for the same sign top pair production via the Z' FCNC couplings.

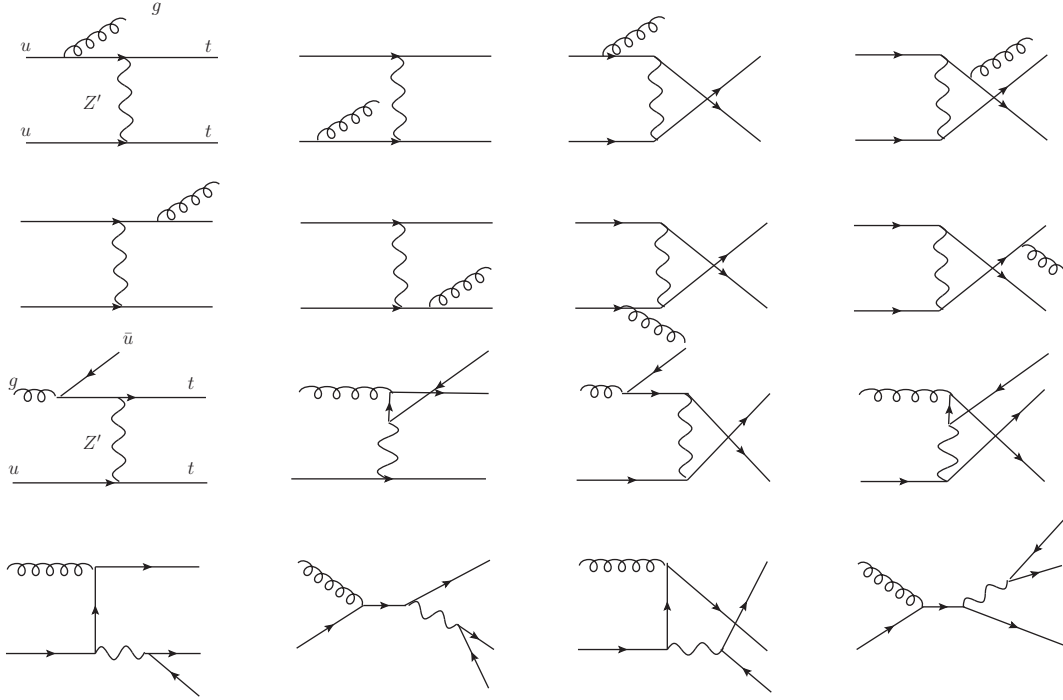


FIG. 13: Feynman diagrams of the real corrections for the same sign top pair production via the Z' FCNC couplings.

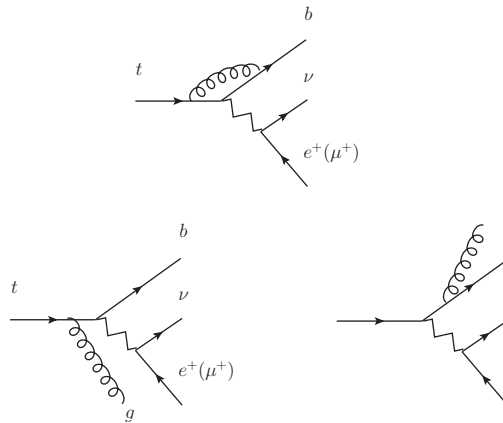


FIG. 14: Feynman diagrams for the top decay at the NLO level.